# SUAS 2026 Technical Design Report

KFUPM ASCENT Team
*College of Engineering and Physics*
*King Fahd University of Petroleum and Minerals*
Dhahran, Saudi Arabia
kfupmascent@outlook.com

***Abstract*—This report documents the design, strategy, and testing of ASCENT-1, an autonomous unmanned aircraft system developed by KFUPM ASCENT for the 2026 Student Unmanned Aerial Systems competition. The team follows a reliability-first strategy that prioritizes the most heavily weighted mission tasks, targeting the Efficient Operators, Risk Mapping, and Search, Detect, and Deliver criteria while accepting a reduced Design for Rapid Response result. ASCENT-1 is built on a modified Aurelia X6 MAX hexacopter running ArduCopter on a Cube Orange Plus, chosen for its motor redundancy, precise low-speed station keeping, and repeatable autonomous takeoff and landing. The onboard autonomy stack runs on a Jetson Orin Nano companion computer that commands the autopilot over a dedicated serial link and executes a verified mission state machine in which every failure path returns the aircraft to launch. Perception uses a Basler global-shutter camera and a YOLO26 model fine-tuned on a self-collected aerial dataset and deployed as a TensorRT FP16 engine, sustaining 7–8 inferences per second within the Jetson's 15 W budget to search the boundary, confirm targets, and georeference them for delivery and for a stitched risk map. Our payload delivery mechanism was chosen from three tested ones due to its reduced weight and low probability of error. Each subsystem was verified in isolation and the integrated aircraft was validated through simulation and full-mission flight rehearsals, in which the localized target settled within roughly two meters of the object on the first pass**

## ACKNOWLEDGMENT

The ASCENT Team expresses its utmost appreciation to its advisors, Eng. Jaber Sahli and Eng. Mohammed Aves, for their technical, logistical and managerial advice, and for helping the team secure required permissions, resources, and facilities. The team would also like to thank former members of KFUPM's UAS2030 team for sharing invaluable advice from their experience in prior SUAS installments, thus helping the team navigate major obstacles. The team greatly thanks its sponsors and partners for their generosity: TASNE3D for providing the team with ample filament to comfortably iterate on designs, T-Motor for providing the team with various propulsion systems components, LightWare for providing the team with state-of-the-art LiDAR technology to help achieve utmost detection accuracy, and Dhahran Techno Valley's Dream Realization Lab for allowing the team to use its equipment to manufacture parts. The team secured funding due to the help and generosity of KFUPM Fund and KFUPM's Aerospace Department; the latter also provided the team with access to facilities in which the development process took place.

## I. COMPETITION STRATEGY

### A. Strategic Vision

Successes and failures faced during the team's numerous hours spent testing in mock missions have made it abundantly clear that any capabilities that have not been exhaustively tested do not reliably demonstrate success and safety in the field. The mission awards a maximum of 1,000 points across five main tasks; however, keeping in mind limited time and flight-test hours, KFUPM ASCENT's strategy prioritizes reliably achieving points in metrics highly weighted in the rubric in lieu of maximizing for all possible achievable points.

Thus, the team's competition strategy is based on the subset of tasks the team's chosen platform can confidently execute, while deliberately disregarding metrics that would award marginal points while requiring disproportionate effort to make reliable.

ASCENT-1, built on a modified Aurelia X6 Max airframe [1] running ArduCopter 4.6.3 [2] on a CubeOrange+ [3], embodies this philosophy. Despite the vehicle's modest endurance class, its mechanical simplicity, motor redundancy capabilities, simple and repeatable autonomous takeoff and landings, precise low-speed station-keeping, and its compatibility with both competition runways map directly onto the aforementioned task prioritization.

### B. Task Prioritization

Due to the availability of experienced operators, the team plans on running the mission with only two operators: a safety pilot and a GCS operator. This maximizes the number of points earned from the Efficient Operators criterion. In order to sufficiently meet this goal without jeopardizing the mission, the team has extensively prepared the platform's autonomous waypoint, landing, and takeoff behaviors. The platform communicates with the ground station using a Herelink (2.4 GHz HD video + control) [4] and an onboard MAVLink2 serial link [5], with Mission Planner serving as the ground control station software. Two air-ground links were evaluated for this role: the Herelink and the SIYI 7 PRO. The Herelink was selected because its open-source software stack allowed the team to stream the AI-annotated detection video directly from the Jetson Orin Nano companion computer to the ground station, giving the safety pilot the same view the detector sees while the aircraft is airborne. The SIYI 7 PRO, by contrast, runs a closed-source stack that provided no supported path for injecting the companion computer's video stream, so the detection overlay could not be carried over that link, a limitation that outweighed the unit's other advantages given how central the live overlay proved to be during field debugging.

Risk Mapping and Search, Detect, and Deliver serve as the team's most prioritized criteria. The stability of the chosen platform and the Jetson-based imaging pipeline aid in producing high-coverage, low-distortion stitched imagery, and the aforementioned stability of the platform allows it to hold in place during the delivery of the payload from above the required height of 150' AGL. The most significant portion of the time spent testing centered around ensuring high map quality and precise payload delivery. For image capture, a Basler a2A5320 — 16 MP (5320 × 3040) global-shutter camera was used [6], and images were processed in an NVIDIA Jetson Orin Nano imaging pipeline [7]. For payload delivery, drops are manually approved before release, after which delivery is handled by a custom-built passive two-stage drop mechanism. This design was selected over a motor-driven winch specifically to remove an active actuator from the descent path: a servo-actuated latch is the only powered element, and the descent itself is governed entirely by gravity and a passive FRT-G2-600 rotary damper acting through a 28 mm braked pulley. The payload deploys through an initial low-resistance stage before the line engages the damped pulley for a controlled final descent. A 25 m–25 m stage split was tested repeatedly across both payload variants, five water-bottle drops and six beacon drops, with a 100 % release success rate and no structural damage in any test, completing the full 50 m deployment in approximately 36 s at an average speed of 1.39 m/s. The mechanism is now being retuned to a 35 m low-resistance stage followed by a 15 m damped stage to shorten total deployment time while preserving sufficient braking distance. The water-bottle (285–335 g) and beacon (220 g) variants share the same frame, release, spool, pulley, line, and damper, differing only in holder and casing geometry, a deliberate commonality choice that halves the number of mechanisms requiring independent qualification.

The UAV has a maximum airtime of up to 70 minutes. Because this number decreases with additional payload, the team prioritized designing with weight in mind. Notable examples include printing with lightweight filaments, such as PLA AERO, and making an effort to topologically optimize any added designs. Thus, the team hopes to achieve as many laps as the battery life allows, and will, if necessary, end before the ideal 10-lap maximum to ensure time to complete the rest of the mission requirements. This, in addition to the aforementioned autonomous landing and takeoff, helps maximize the number of points the team may earn by not designing for complete fulfillment of the Flight Endurance criterion.

In order to maximize points earned in other criteria, the team plans to compromise the possible points earned from the Design for Rapid Response criterion. The platform's weight and volume, in addition to its complexity, take away from the possible points to be earned during the mission. Despite this, the system still maintains the below 100Wh battery mark, earning the team 75 points.

## II. Design Strategy

### A. *Airframe and Propulsion*

Three airframe options were previously considered before ASCENT's design cycle: an in-house quadcopter, a fixed-wing VTOL, and a modifiable commercial hexacopter platform adapted to the team's requirements. The in-house quadcopter was dismissed first. With only four motors, the loss of a single motor is unrecoverable, a risk the team was unwilling to carry given our emphasis on reliability, and the design and fabrication effort required would have drawn hours away from the custom perception and payload-delivery development that the team judged more critical to its overall strategy. A fixed-wing VTOL remained under consideration longer, given its potential to substantially extend endurance beyond what a multi-rotor can achieve. However, the mission's 45-minute time limit was already comfortably met by simpler airframes under evaluation, and the endurance advantage did not justify the added cost of a dual-mode flight controller, the additional pilot training required for the transition phase, or the larger footprint the airframe would present during deployment. Ultimately, we decided to continue to modify the Aurelia X6 MAX airframe. Its six-motor configuration was the primary factor in this decision: the aircraft remains flight-capable on five motors, which removes the single-point-of-failure inherent to the quadcopter option. Its 15.6 kg maximum takeoff weight provides sufficient margin to carry the payload delivery hardware and companion computer without operating near the airframe's structural limit, and its rated 70-minute flight time affords a substantial buffer over the 45-minute mission window once the additional draw of the vision and delivery subsystems is accounted for.

Motor selection followed similar evaluation. High-KV motors typical of racing platforms were considered but ruled out because such motors are optimized for high rotational speed rather than the low-speed, high-torque hover performance the mission demands. Lower cost motors were considered, but thrust output between individual units could not ensure consistent performance across six motors, and this variability was deemed an unacceptable risk. The team selected the T-Motor MN6007II 320KV motor paired with Hobbywing Platinum V4 60A electronic speed controllers. The MN6007II's lower KV rating and larger stator provide greater torque at reduced RPM, improving hover efficiency at the vehicle's loaded weight.

Battery selection was governed by three simultaneous requirements: sufficient total pack energy to complete the 45-minute mission with reserve, fulfillment of the *Easy to Transport Batteries* criterion, and adequate continuous discharge current to supply six motors without excessive voltage sag under load. LiPo cells, used extensively in drone systems,

Fig. 1. Profile of ASCENT-1 drone.

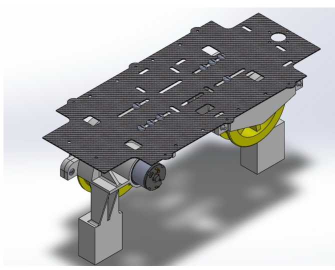

Fig. 2. Brushed DC Motor Design

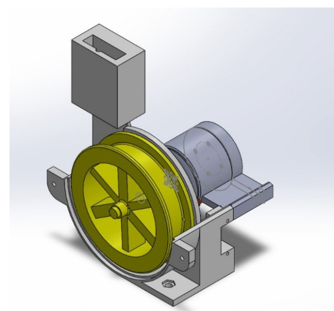

Fig. 3. BLDC Payload Delivery Mechanism

were considered but not used. The high discharge rate that LiPo offers is of limited benefit once current draw is shared across six motors, whereas the higher energy density of li-ion cells offers a more direct benefit to a mission focusing on slower search, mapping and hovering rather than racing. The team selected the MaxAmps 6S 97.2 Wh lithium-ion pack, with eleven packs wired in parallel. Each individual pack remains under the 100 Wh threshold required for the team's transport classification, and distributing current draw across eleven packs rather than one reduces the discharge demand placed on any single pack, improving thermal margin and limiting the impact of a single degraded pack on overall flight capability.

### B. Payload Delivery

Three payload delivery systems were simultaneously developed: a winch design dependent on a brushed DC motor, a winch design dependent on a brushless DC motor, and finally, a motorless rotary-damper design.

*1) Brushed DC Motor Design:* The design utilizes a brushed DC motor to drive the winch mechanism and safely deploy the payload. A brushed-gear motor was selected to deliver high mechanical torque at low speeds using a highly reliable two-wire interface. The motor mounts directly to a custom 3D-printed chassis that integrates a vertical landing leg to guarantee adequate ground clearance for the suspended load. A protective shroud encloses the 80-millimeter outer diameter spool to retain the line securely and block heavy rotor downwash during aggressive flight maneuvers. A BTS7960 H-bridge module acts as the primary motor driver. An Arduino Nano generates precise pulse-width modulation signals for this driver to dynamically regulate the spool speed. This electrical architecture allows the aircraft to lower the payload smoothly under high-level commands from the main NVIDIA Jetson Orin Nano companion computer. The Arduino handles all real-time timing to prevent uncommanded drops if the main computer experiences a software delay. A custom two-layer carrier printed circuit board physically separates the 12-volt motor power bus from the sensitive 5-volt logic rail to stop electrical noise from resetting the microcontroller during a heavy lift. The structural housing and spool are printed using PLA filament to maintain strict rigidity. The entire bare payload subsystem weighs approximately 800 grams. The complete mirrored assembly is shown in Fig. 2.

*2) BLDC Motor Design:* The second alternative considered relies on a BLDC Motor to drive the winch mechanism and deliver the payload. In order to sufficiently drive a heavy enough load, a BLDC Motor with a lower KV value was selected; in this case, a T-Motor MN3508 380KV unit was selected as a primary option, offering a lightweight option along with a low KV value. Alternatively, a SunnySky X4112S 400KV is used due to its availability in the team's workspace.

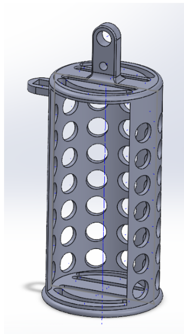

Fig. 4. Bottle Holder

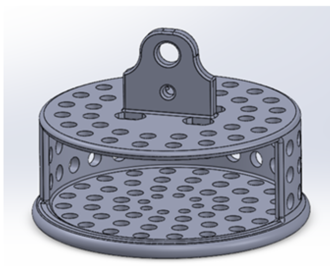

Fig. 5. Beacon Holder

The motor is attached to a 5:1 planetary gearbox: a compact attachment allowing the motor to hold the payload in space completely suspended, with no need for a servo to actuate the drop. An Electronic Speed Controller (ESC) connected to the Jetson Orin Nano Board is used to dynamically control the speed of the motor, allowing the motor to spin faster at higher altitudes and slower at lower ones for added safety. This allows the drop to max out at approximately 4 meters per second (assuming an 80mm diameter pulley and a 12V Battery) allowing it to complete the drop in 15-30 seconds at an altitude of 150' AGL. The holder is printed with PLA as it is a strong, lightweight filament. The complete assembly's weight ranges from 835.82 - 967.82 grams, depending on the motor used. The final design is shown in Fig. 3.

*3) Passive Two-Stage Rotary-Damper Design:* The third alternative considered utilizes a passive two-stage rotary damper to lower the payload without relying on a motor-driven winch. The design uses gravity to release the payload rapidly during an initial low-resistance free-fall stage and a rotary damper to reduce its speed during a final stage, removing the need for continuous electronic control during the drop. The mechanism is designed for a total deployment distance of approximately 50m. The selected operating sequence consists of an initial 35m low-resistance free-fall stage and a final 15m rotary-damper-controlled descent stage. The term free fall in this design describes the low-resistance deployment stage. The payload is still connected to the aircraft by the payload line, and its movement is affected by spool resistance, line friction, aerodynamic drag, and the geometry of the payload casing. Therefore, it is not treated as an ideal unrestricted free fall. Two versions of the mechanism were manufactured. The first carries the water bottle, while the second carries the electronic beacon. Both versions use the same structural frame, release mechanism, free-fall spool, braked pulley, payload line, and rotary damper. Only the payload holder and protective casing are different.

The payload drop mechanism consists of a 3D-printed structural frame, servo-actuated release, free-fall line spool, braked pulley, FRT-G2-600 rotary damper, payload tether line, and a payload-specific holder/casing. Before deployment, a servo-actuated latch retains the payload inside its holder; on the release command, the servo moves the retaining component and releases the payload. The mechanism carries either a water bottle (200–250 mL, cylindrical casing) or an electronic beacon (smaller, form-fitted casing), with both using the same braking and release system.

Deployment occurs in two stages. The free-fall spool releases line with low resistance as the payload moves rapidly away from the aircraft. Once the second line section engages, the braked pulley rotates the FRT-G2-600 rotary damper, whose resistance slows the pulley and the payload. The damper is not the sole source of resistance – pulley, bearing, and line-guide friction, spool resistance, aerodynamic drag, line elasticity, and progressive stage engagement all contribute. For this reason, evaluation relied mainly on physical testing of the complete assembly rather than nominal damper torque.

The braked pulley has an effective diameter of 28 mm, giving

$$r_p = \frac{D_p}{2} = \frac{28}{2} = 14 \text{ mm}. \tag{1}$$

Line speed $v$, pulley diameter $D_p$, and rotational speed $n_p$ are related by

$$n_p = \frac{60v}{\pi D_p}, \tag{2}$$

useful for future testing once line speed is measured, though final design was selected from observed performance rather than this theoretical relation alone.

Several successful tests used a 25 m initial stage and a 25 m braked stage. The payload released, cleared the mechanism, deployed both line sections, transitioned into a slower descent, and reached the ground operator at a controlled speed. The full 50 m deployment took approximately 36 s, giving an average speed of

$$v_{\text{avg}} = \frac{H}{t} = \frac{50}{36} \approx 1.39 \text{ m/s}, \tag{3}$$

though this overall average masks the faster first stage and considerably slower braked stage. No damage or injury was observed, confirming sufficient braking for the tested conditions.

Based on these results, the mechanism is being reconfigured to a 35 m initial stage and 15 m braked stage, to reduce total deployment time while retaining enough braked distance for

Fig. 6. Passive Two-Stage Rotary-Damper Design

adequate speed control. This arrangement, applicable to both the water-bottle and beacon versions, will be verified through further ground testing before competition use.

*4) Mechanism selection:* The passive two-stage rotary-damper mechanism was selected over alternative designs on the basis of repeated physical drop testing rather than analytical prediction alone. Because the final braking response depends on the combined behavior of pulley friction, bearing friction, line-guide friction, spool resistance, aerodynamic drag, line elasticity, and the rotary damper itself, the complete assembly was tested as a single system instead of characterizing the damper in isolation. This approach was chosen specifically to validate that the mechanism, as a whole, would behave predictably under real deployment conditions rather than relying on nominal damper torque values that would not capture these secondary effects.

Testing was structured to confirm reliable servo release, smooth line deployment, proper transition between stages, correct line tracking within the pulley grooves, controlled descent speed during the braked stage, safe payload reception, and to allow inspection of the frame, pulley, casing, and line after each test.

The 25 m–25 m configuration was tested repeatedly to establish confidence in the mechanism before committing to a final stage arrangement. Across these tests, the mechanism consistently completed full deployment, the payload reliably slowed upon engagement of the rotary-damper pulley, and no structural damage was observed, supporting the decision to retain this mechanical architecture for competition use. The total drop time was approximately 36 s.

With the two-stage principle validated, the mechanism was further tested at the selected 35 m–15 m configuration for both payload variants to confirm that the design choice would generalize across payload masses. The results of this final validation are summarized in Table I.

The 100% release success rate for both payloads, combined with the absence of structural damage across all trials, confirmed that the same frame, release mechanism, free-fall spool, braked pulley, and rotary damper could reliably support both payload configurations without modification beyond the holder and casing. These results were the basis for finalizing the 35 m–15 m configuration ahead of final competition validation.

TABLE I
PAYLOAD DROP TEST RECORD

| Measured Parameter | Water Bottle | Beacon |
|---|---|---|
| Initial-stage distance (m) | 35 | 35 |
| Braked-stage distance (m) | 15 | 15 |
| Total drop time (s) | 36 | 32 |
| Release success rate (%) | 100 | 100 |
| Number of successful tests | 5 | 6 |
| Final structural condition | Undamaged | Undamaged |

*5) Payload Holders:* The final water bottle holder (Fig. 4) is a topologically optimized cylindrical cage that pairs a perforated lattice wall with a load-bearing skeleton, cutting roughly 40% of the structural mass while preserving a payload bay sized to accept the full range of anticipated bottle diameters and a mounting lug that aligns cleanly with the drop mechanism. The final beacon holder (Fig. 5) is a low-profile cylindrical housing built around a reinforced impact-attenuating base that absorbs landing energy and shields the electronics on ground contact, with an aggressively perforated shell and floor that trim over 40% of the mass and a refined mounting tab that seats correctly in the release mechanism. Both components are cleared for flight and operational testing.

### *C. Avionics*

The core architecture of our UAV (Fig. 7) is centered around an Orange Cube+ flight controller running ArduCopter. The Orange Cube+ was specifically selected for its powerful dual-core processing and triple-redundant IMUs, which mitigate the risk of sensor failure by allowing the system to automatically utilize a healthy backup IMU. For search and risk mapping, it utilizes a Here3+ GNSS module alongside a downward-facing LiDAR rangefinder [8] to ensure accurate navigation and altitude reading. A single HereLink Air Unit was chosen to allow RC control via SBUS, MAVLink telemetry, and low-latency HD video transmission into a 2.4 GHz digital data link.

### *D. AI Search, Classification and Mapping*

The Nvidia Jetson Orin Nano is utilized as the onboard computer, communicating with the flight controller via a MAVLink UART connection. The Orin Nano was selected for its high TOPS capability at a low power draw, enabling efficient AI processing of visual data. It executes perception and mission logic and commands the Cube Orange+ autopilot over a dedicated MAVLink2 serial link. Mission execution is governed by an explicit state machine with the states INIT, SEARCH, CONFIRM, COMMIT, LOITER, and RTL. Each transition requires verified preconditions: the waypoint mission is read back from the autopilot before AUTO is engaged, and every commanded mode change is confirmed against the flight controller heartbeat before the mission advances. Any state timeout or loss of the companion process triggers an autonomous return-to-launch. The companion computer is assigned a dedicated MAVLink system identifier so that ArduPilot's ground-station failsafe monitors the Jetson specifically. This structure allows the vehicle to perform the Search,

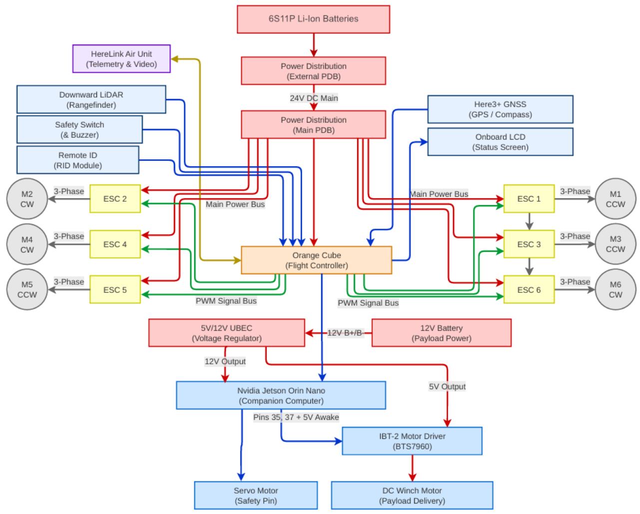


Fig. 7. Electrical architecture of ASCENT-1

Detect, and Deliver task with the minimum two-operator crew and to attempt fully autonomous takeoffs and landings.

The Search Boundary is covered by an ArduCopter AUTO mission generated on board from the four surveyed corner coordinates, with the lane spacing computed from the camera ground swath at the 150' AGL search altitude and a 30% overlap. The parameter WP_YAW_BEHAVIOR is set to 0 so the vehicle holds a fixed heading and translates through each lane reversal, preserving ground speed and a constant camera orientation. The Basler ace camera streams 5320 x 3040 global-shutter frames to the Jetson, where a producer-consumer design copies the raw Bayer frame in the capture thread and runs inference on the most recent frame. Detection and classification are performed by a YOLO26 network deployed as a TensorRT FP16 engine at approximately eight inferences per second, and a detection is accepted only after three results above a 0.5 confidence threshold occur within the five most recent frames.

Each accepted detection is georeferenced by projecting the detection pixel through the camera intrinsics, rotating it by the aircraft attitude at the frame timestamp, and intersecting it with the ground plane. The estimate is refined in the LOITER state until the standard error of the mean falls below 3 m. The converged coordinates feed the delivery targeting, and the same nadir imagery is orthorectified and stitched into the georeferenced map for the Risk Mapping task.

## III. Testing Strategy

To ensure the reliability of our UAV in performing mission tasks, a multi-stage testing process was used. Early stages began with testing of all individual candidate components for the UAV's main subsystems before testing of complete subsystems. Afterwards, the entire system was tested using HITL and SITL simulations before complete flight tests were performed within safe, open premises. The results of each testing stage informed design decisions made during team-wide meetings that discussed the ability of individual components or subsystems in integrating with other subsystems, handling operational limits, and ensuring the entire system will fulfill the strategic goals outlined in Section I.

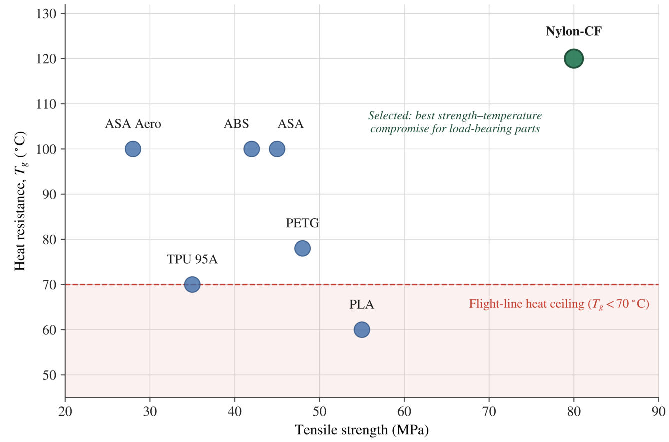


Fig. 8. Material selection by heat resistance against mechanical strength for each printed part.

### A. Component Testing

Individual components were extensively tested during the early stages to ensure their health and reliability. Tests were performed to extract four key pieces of information: agreement on performance with manufacturer specifications, identification of operational limits, consistency of operation, and compatibility with other components.

**Airframe and Propulsion.** Thrust, current, and endurance were modeled in eCalc [9] at the competition weight and battery. These were then checked against measured power draw in early flights to confirm adequate margin at the full loaded weight. Motor-out behavior, vibration, and compass calibration were verified on the assembled aircraft before autonomous flight.

**Payload Delivery Mechanism.** Each winch drive was run on the bench to confirm controlled line pay-out and to verify that the microcontroller timing prevents an uncommanded drop during a main-computer delay. The lowering rate was measured against the design target of approximately 4 m/s, yielding a 15 to 30 second drop from the 150' AGL release altitude. Repeated drops confirmed line retention under rotor downwash.

**Payload Holders and Materials.** Materials were matched to the heat and load each part must survive in flight (Fig. 8). The topology-optimized holders were printed to cut roughly 40% of structural mass while preserving fit. Each holder was verified to seat correctly in the release mechanism and to accept the full range of anticipated bottle diameters. The beacon housing's impact-attenuating base was tested for landing-energy absorption.

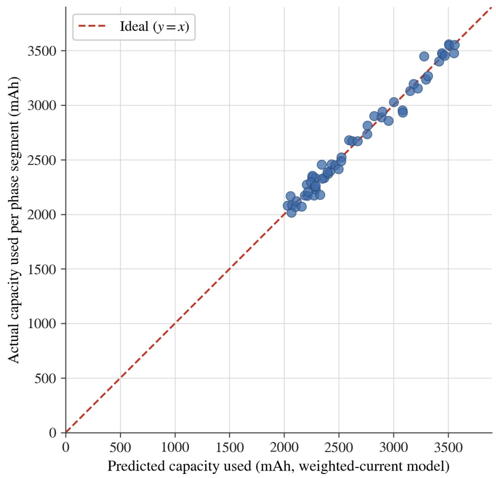


Fig. 9. Predicted against actual battery usage per flight segment; points near the one-to-one line show the model tracking real consumption.

**Power, Battery, and Avionics.** The energy model predicting per-segment battery use was validated against logged flights. Predicted energy tracked the measured milliamp-hours closely and drifted slightly high on the longest segments, which is the conservative direction for endurance planning (Fig. 9). The battery configuration was checked against the mission energy budget and the transport packaging limit. The Cube Orange+ redundant IMUs, the Here3+ GNSS, and the downward LiDAR rangefinder were verified through calibration and stable navigation and altitude hold in flight.

**Communication and Failsafes.** The MAVLink2 link was tested in each direction independently. This followed an early fault where downlink telemetry arrived while uplink commands were lost, which was traced to a dead transmit pin and corrected. Mode changes are confirmed against the flight controller heartbeat, and mission uploads are accepted only after the stored item count is read back. The companion-computer failsafe was verified in flight by terminating the mission process and confirming an autonomous return-to-launch.

**Perception and Localization.** The detector was benchmarked on the Jetson Orin Nano at its 15W setting, yielding a per-frame latency near 150 ms for the YOLO26-L engine and approximately 8 detections per second (Fig. 10). It was evaluated on imagery at flight-realistic altitude and scale. The three-of-five confidence-gated debounce was tested against isolated false positives. Georeferencing was verified by pairing each detection with the vehicle pose at its frame timestamp and refining the estimate in a LOITER orbit to a bounded standard error.

### B. Mission-Level Validation

*1) Simulation:* Real flights are costly, weather-dependent, and impossible to repeat exactly across the hundreds of scenarios needed to trust a search strategy. Therefore, the search planner was first evaluated in a purpose-built simulator. It is

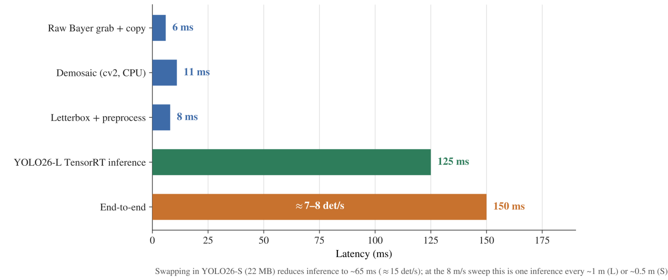


Fig. 10. Per-frame latency budget on the Orin Nano at 15 W; inference dominates and the remaining stages are kept cheap.

structured as a layered pipeline with one-way dependencies from the mission map down to the metrics: Map Parser, World Model, Drone Model, Camera Model, Coverage Engine, Simulation Engine, Search Algorithm, and Evaluation Framework. The official RoboNation KML [10] is parsed directly into a local ENU frame, preserving the true flight boundary, both search boundaries, the runways, and the operational areas. The drone model enforces aircraft speed and motion limits, and the camera model defines the ground footprint at altitude. The central design decision tracks coverage geometry (which ground was imaged) separately from detection (whether a target in that area was actually seen). The detection stage accounts for occlusion, image resolution, and range, allowing a planner to be scored on what it would detect rather than on the ground it overflew. Every search algorithm implements a common interface, so new strategies are added without altering map handling, simulation, or scoring. The competition flight software is deliberately excluded from the core and connected only through edge adapters. Each run is scored on completion time, time to first detection, distance, energy, coverage, coverage efficiency, redundant coverage, turns, and success rate. Algorithms are compared at scale through seeded Monte Carlo campaigns of 1,000 missions each at 45.72 m (150’) AGL, with a 10 m cell, 18 m/s, a 120 Wh budget, and a 70° horizontal field of view, plus a one-at-a-time sensitivity study. Ranking stability is assessed by mean rank and its standard deviation across configurations (Fig. 11). In these preliminary campaigns, the deterministic lawnmower pattern led on both efficiency and consistency. Probabilistic planners are still being implemented, so no final selection has been made.

*2) Flight Testing:* The integrated stack was validated in full-mission rehearsals on ASCENT-1, flown against the same corner coordinates used in simulation. The committed target position settled within approximately 2 m of the object on the first pass, consistent with the convergence bound enforced in the LOITER state. The payload mechanism accordingly performed within the required ranges (Fig. 12). The search, confirmation, commit, and return-to-launch transitions executed in sequence on the real aircraft. These flights also supplied the logged power data used to validate the energy model and confirmed the link and failsafe behavior under real

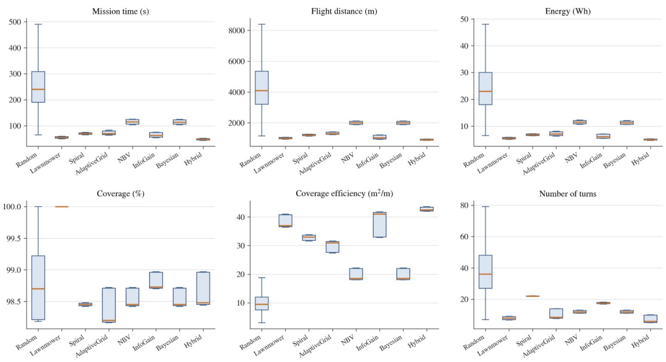


Fig. 11. Monte Carlo comparison of search algorithms across mission-completion metrics on the official SUAS 2026 environment.

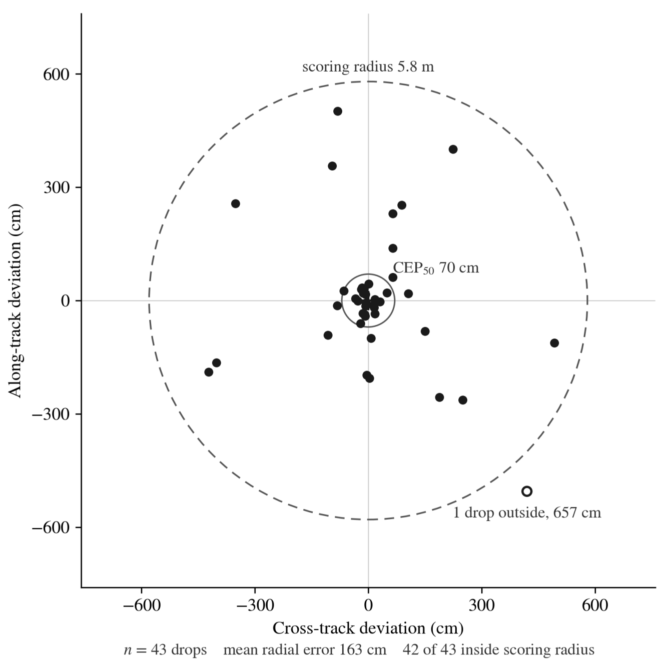


Fig. 12. Payload drop accuracy plot.

radio conditions.

## REFERENCES

[1] Aurelia Aerospace, "Aurelia X6 MAX — heavy lift payload drone," product documentation. [Online]. Available: https://aurelia-aerospace.com/products/aurelia-x6-max

[2] ArduPilot Dev Team, "Copter documentation (ArduCopter)," [Online]. Available: https://ardupilot.org/copter/

[3] CubePilot, "The Cube Orange+ overview," [Online]. Available: https://docs.cubepilot.org/user-guides/autopilot/the-cube-module-overview

[4] CubePilot, "Herelink overview," [Online]. Available: https://docs.cubepilot.org/user-guides/herelink/herelink-overview

[5] MAVLink Development Team, "MAVLink developer guide," [Online]. Available: https://mavlink.io/en/

[6] Basler AG, "Basler ace a2A5320-23ucBAS area scan camera," [Online]. Available: https://www.baslerweb.com/en/shop/a2a5320-23ucbas/

[7] NVIDIA Corp., "Jetson Orin Nano developer kit," [Online]. Available: https://developer.nvidia.com/embedded/jetson-orin

[8] LightWare LiDAR, "LiDAR distance measurement sensors," [Online]. Available: https://lightwarelidar.com/

[9] M. Müller, "eCalc — xcopterCalc multicopter calculator," [Online]. Available: https://www.ecalc.ch/xcoptercalc.php

[10] RoboNation, "SUAS 2026 team handbook," [Online]. Available: https://robonation.gitbook.io/suas-resources/2026-team-handbook